



Hydrogenolysis of glycerol to propylene glycol in continuous system without hydrogen addition over Cu-Ni catalysts



Isabelle C. Freitas, Robinson L. Manfro, Mariana M.V.M. Souza*

Escola de Química – Universidade Federal do Rio de Janeiro (UFRJ), Centro de Tecnologia, Bloco E, sala 206, CEP 21941-909, Rio de Janeiro, RJ, Brazil

ARTICLE INFO

Article history:

Received 18 January 2017

Received in revised form 2 August 2017

Accepted 8 August 2017

Available online 12 August 2017

Keywords:

Glycerol

Hydrogenolysis

Propylene glycol

Nickel

Copper

ABSTRACT

A series of Cu, Ni and Cu-Ni catalysts with 20 wt% of each metal, supported on Al_2O_3 and ZSM-5, was prepared by wet impregnation method and tested in glycerol hydrogenolysis to 1,2-propanediol (propylene glycol) using a WHSV of 2 h^{-1} at 250°C , and pressure of 40 bar for 6 h. Without external hydrogen, the reaction pathway involves glycerol dehydration to acetol, with simultaneous reforming to H_2 and CO_2 ; this hydrogen generated *in situ* is used for the hydrogenation of acetol to propylene glycol. Under these conditions, the CuNi/ Al_2O_3 and CuNi/ZSM-5 catalysts exhibited the highest glycerol conversion, 80% and 85%, respectively, with propylene glycol yield around 25%. With external hydrogen, all catalysts showed higher glycerol conversion (>90%) and the monometallic Cu catalysts presented higher conversion to liquid and propylene glycol yield than the bimetallic ones; the Cu/ Al_2O_3 showed the highest yield to propylene glycol (70%). The activity of the catalysts was correlated with their metallic dispersion and also the support acidity.

© 2017 Elsevier B.V. All rights reserved.

1. Introduction

Fossil fuels are currently the largest source of energy in the world; however, their extensive use leads to the increase of carbon dioxide concentration in the atmosphere. Due to this fact, concern about the environment has been growing and the environmental laws are becoming more stringent. Besides the environmental issue, another serious problem is the reduction of oil reserves. Despite the discovery of new oil fields, this is a source of finite energy. For these reasons, researchers are looking for alternative energy sources. One of the alternatives to fossil fuels is biomass that could eventually replace oil.

Several high value-added products and fuels can be obtained from biomass: biogas that is obtained from the waste, bio-oil obtained from the pyrolysis reaction, bioethanol from lignocellulosic material, as well as biodiesel, the most popular among others, which is obtained by transesterification reaction of vegetal oils or animal fats. In the production of biodiesel, glycerol is obtained as a byproduct of the transesterification reaction: one ton of biodiesel results in around 110 kg of crude glycerol, or 100 kg of pure glycerol [1].

The use of glycerol as a feedstock for the production of high value-added products is very interesting due to its high availability and low price in the market. Several products can be obtained from glycerol, such as 1,3-propanediol, 1,2-propanediol, β -carotene, propionic acid, epichlorohydrin, ethanol, syngas, and hydrogen [2]. 1,2-propanediol or propylene glycol has an average value in the market of 1.0–2.2 \$/kg and has an annual growth of 4% [3,4]. Propylene glycol is used as feedstock to produce polyester resin, liquid detergent, pharmaceuticals, cosmetics, and paints [4]. Traditionally it is obtained by hydration of propylene oxide [3].

Propylene glycol is obtained from glycerol by hydrogenolysis reaction that involves breaking of $\text{C}=\text{O}$ chemical bond and the simultaneous addition of hydrogen [3]. The most commonly used heterogeneous catalysts for the hydrogenolysis reaction are the noble metals, such as Pt, Rh, Ru, Pd, Ir, and Re, because they exhibit high selectivity to propylene glycol and a high conversion of glycerol [3–6]. However, non-noble metals, such as Cu, Co, and Ni, can present catalytic activity as high as noble metal catalysts, besides having lower cost [1,7–10].

Nickel-based catalysts have high activity for producing hydrogen since they are typical catalysts for glycerol reforming, which is an advantage for the hydrogenolysis reaction, because there is no need for external addition of hydrogen to the system [1,4]. As hydrogen is usually derived from fossil fuels, the use of hydrogen generated *in situ* from glycerol reforming turns hydrogenolysis into a more “green” process.

* Corresponding author.

E-mail address: mmattos@eq.ufrj.br (M.M.V.M. Souza).

In the literature there are few studies on the glycerol hydrogenolysis without using external hydrogen; most of them with batch reactors. D'Hondt [11] reported that Pt/Al₂O₃ catalyst exhibited 99.9% of glycerol conversion and 19.1% of propylene glycol selectivity at 230 °C, in a batch reactor, under inert atmosphere. Roy et al. [12] tested a mixture of Ru and Pt catalyst supported on alumina, also using a batch reactor, and obtained 50% of glycerol conversion and 47% of propylene glycol selectivity, at 220 °C, under 14 bar of N₂ pressure. Yun et al. [13] studied bimetallic Cu-Ni catalysts supported on mesoporous alumina for glycerol hydrogenolysis in a batch reactor, obtaining 60% of glycerol conversion and 20% of propylene glycol yield at 220 °C, under atmospheric pressure. More recently, Seretis and Tsakaras [14] studied aqueous phase reforming and hydrogenolysis of glycerol in a batch reactor, using 65%Ni catalyst supported on SiO₂/Al₂O₃; the maximum propylene glycol yield was 22% after 4 h of reaction at 240 °C, under autogenous pressure. The only report of continuous operation, without H₂ addition, was that of Mane and Rode [15], using Cu-Al catalyst prepared by co-precipitation, obtaining 90% of glycerol conversion, 25% of propylene glycol and 55% of acetol selectivities, at 220 °C under 20 bar of N₂ pressure. Rajkhowa et al. [16] studied glycerol hydrogenolysis with Cu/Al₂O₃ catalyst in an isothermal trickle-bed reactor at 230 °C, with very high selectivity to propylene glycol (94.7%), but using high hydrogen pressures (80 bar).

In this work, Cu, Ni and Cu-Ni catalysts supported on Al₂O₃ and ZSM-5 were employed for glycerol hydrogenolysis in continuous reactor, using hydrogen generated *in situ* and also with the addition of external hydrogen. The continuous operation of hydrogenolysis reactor is not common in the literature, and most of the works only use external hydrogen. Therefore, our goal here is to investigate the influence of the metal, the support nature and the effect of hydrogen in the catalytic performance for glycerol hydrogenolysis to propylene glycol.

2. Experimental

2.1. Catalyst preparation

Cu, Ni and Cu-Ni catalysts supported on HZSM-5 (FCC) and Al₂O₃ (BASF) were prepared using the wet impregnation method, with CuO and NiO loading of 20 wt%. In a typical preparation, Cu(NO₃)₂·6H₂O and Ni(NO₃)₂·6H₂O (Sigma-Aldrich) were dissolved in deionized water, and a known amount of powdered support was added afterward. After 2 h of rotation for homogenization, the water was removed by evaporation at 80 °C under vacuum. Finally, the obtained material was dried at 110 °C for 12 h, and calcined at 500 °C for 3 h under air flow (60 mL min⁻¹). The prepared catalysts will be referred to as Cu/Al₂O₃, Ni/Al₂O₃, CuNi/Al₂O₃, Cu/ZSM-5, Ni/ZSM-5 and CuNi/ZSM-5.

2.2. Catalyst characterization

The chemical composition of the catalysts after calcination was determined by X-ray fluorescence (XRF) using a Rigaku Primini spectrometer, with X-ray generator tube of palladium.

X-ray diffraction (XRD) was carried out on a Rigaku Miniflex II diffractometer with CuK α radiation (30 kV and 15 mA). The measurements were performed with steps of 0.05° using a counting time of 1 s per step and over the 2θ range of 5°–90°. Reduced catalysts were analyzed after *ex situ* reduction under the same conditions used before the catalytic tests and spent catalysts were analyzed without any other treatment after reaction. The average diameter of the Cu, Ni and Cu-Ni crystals was calculated by

Scherrer equation (Eq. (1)), using the diffraction peak correspondent to (111) plane:

$$d = \frac{k\lambda}{\beta \cdot \cos\theta} \quad (1)$$

where d is the average diameter of the crystals (Å), k is a constant that depends on the particle shape (for sphere, k=0.94), λ is the wavelength of the X-ray source (for CuK α , λ=1.5488 Å), β is the full width at half maximum (FWHM) in radians and θ is the diffraction angle. The corresponding metallic dispersion (D) was estimated according to Anderson [17] (Eq. (2)):

$$D = \frac{6V_m}{d \cdot A_m} \quad (2)$$

where V_m is the atomic volume (0.0118 nm³ for Cu and 0.0109 nm³ for Ni), d is the crystallite size (in nm) and A_m is the surface area of a single atom (0.068 nm² for Cu and 0.0649 nm² for Ni).

X-ray photoelectron spectra (XPS) were recorded using a hemispherical spectrometer (PHOIBOS 150 – SPECS) equipped with an X-ray Gun (XR-50) and an Al K α source (soft X-ray source at 1486.6 eV, which is non-monochromatic). The binding energy shifts due to surface charging were corrected using the C 1s level at 284.6 eV, as an internal standard. The spectra were fitted using CasaXPS Version 2.3.16. The base pressure in the analysis chamber was maintained at 5 × 10⁻¹⁰–1 × 10⁻⁹ mbar. Reduced catalysts were analyzed after *ex situ* reduction under the same conditions used before the catalytic tests.

Absorption spectra were obtained by Fourier transform infrared spectroscopy (FTIR) in order to verify the changes in the structure of HZSM-5. A Shimadzu spectrometer, PRESTIGE-21 model, was used to obtain infrared spectra in the region 4000–400 cm⁻¹. The samples were prepared by diluting 3 wt% of the zeolite in KBr (dispersing agent).

N₂ adsorption-desorption experiment was carried out at -196 °C using a Micromeritics TriStar 3000 equipment. The samples were outgassed for 24 h at 300 °C. The specific surface area was obtained using the BET method and pore volume by the BJH method.

The reduction profiles of the catalysts were obtained by temperature-programmed reduction (TPR). The analysis was performed in a conventional apparatus equipped with a thermal conductivity detector (TCD). All samples were pre-treated for 30 min at 150 °C under Argon flow (30 mL min⁻¹). After cooling, they were heated from room temperature to 1000 °C at a heating rate of 10 °C min⁻¹ and a flow rate of 30 mL min⁻¹ of 1.8% H₂/Ar.

The catalyst acidity was investigated by temperature-programmed desorption of ammonia (NH₃-TPD), which was performed using a mass spectrometer QMG-200 Prisma Plus (Pfeiffer). The samples were firstly reduced *in situ* using a mixture of 1.8% H₂/Ar (30 mL min⁻¹) and heating up to 1000 °C (10 °C min⁻¹) for 30 min. Then, the samples were cooled down to room temperature using He. The ammonia adsorption was carried out at 70 °C using a mixture of 4% NH₃/He with a flow rate of 30 mL min⁻¹ for 30 min. After the adsorption, the sample was purged with flowing He at 70 °C for 1 h. The desorption of the chemisorbed ammonia was carried out by heating the samples up to 800 °C at a rate of 20 °C min⁻¹. The ratio m/z=15 was used for quantification of ammonia.

2.3. Hydrogenolysis of glycerol

The glycerol hydrogenolysis was carried out in a fixed bed reactor of Inconel 625, with internal diameter of 0.5 cm. The catalysts in the form of pellets were reduced *in situ* at temperature determined by TPR analysis (550 °C, for Cu-containing catalysts, or 850 °C), for 1 h. The aqueous solution of glycerol (10 vol%) was injected to

the reactor by an HPLC pump (Eldex 1SAM), and the flow rate ($0.041 \text{ mL min}^{-1}$) was adjusted to obtain a weight hourly space velocity (WHSV) of 2 h^{-1} , using 1.25 g of catalyst. The standard reaction conditions were: 250°C , 6 h of reaction and 40 bar of N_2 or H_2 . N_2 or H_2 flow of 30 mL min^{-1} was added through time in order to keep a stable pressure, controlled by a diaphragm-type back pressure regulator.

The product stream from the reactor passed through a heat exchanger at 10°C resulting in the separation of liquid and gas phases. The liquid products were analyzed in a Shimadzu Prominence HPLC with Bio-Rad Aminex HPX-87H column ($300 \times 7.8 \text{ mm}$) at 30°C , using $0.01 \text{ M H}_2\text{SO}_4$ as eluent at 0.6 mL min^{-1} , and refractive index (RID) and ultraviolet (UV) detectors. The identification of compounds was performed by injections of sample standards of glycerol, propylene glycol, acetol (2-hydroxyacetone), ethanol, and acrolein, with construction of a calibration curve for each compound. 1,3-propanediol, ethylene glycol, 1-propanol and 2-propanol were also injected but they were not detected in any reaction. The gas phase was analyzed by a gas chromatograph (GC) Shimadzu GC-2014, equipped with two columns (RtQ-PLOT and Carboxen 1010) and two detectors: thermal conductivity (TCD), for H_2 , CO and CO_2 and flame ionization (FID), for CH_4 analysis, using He as the carrier gas. The column oven was maintained at 40°C for 20 min and then heated at $10^\circ\text{C min}^{-1}$ up to 120°C , for 10 min, resulting in total analysis time of approximately 38 min. The carbon mass balance was greater than 96% for all activity tests.

The glycerol conversion, conversion to liquid, selectivity and yield of propylene glycol, acetol, ethanol and acrolein were calculated according to Eqs. (3)–(6).

$$X(\%) = \frac{C_{\text{C}_3\text{H}_8\text{O}_3}^0 - C_{\text{C}_3\text{H}_8\text{O}_3}}{C_{\text{C}_3\text{H}_8\text{O}_3}^0} \times 100 \quad (3)$$

$$X_L(\%) = \frac{C_{\text{Acetol}} + C_{\text{Propyleneglycol}} + C_{\text{Ethanol}} + C_{\text{Acrolein}}}{C_{\text{C}_3\text{H}_8\text{O}_3}^0} \times 100 \quad (4)$$

$$S_i^l(\%) = \frac{C_i}{C_{\text{Acetol}} + C_{\text{Propyleneglycol}} + C_{\text{Ethanol}} + C_{\text{Acrolein}}} \times 100 \quad (5)$$

$$Y_i^l(\%) = \frac{X_L(\%) \times S_i^l(\%)}{100} \quad (6)$$

where $X(\%)$ is glycerol conversion, $C_{\text{C}_3\text{H}_8\text{O}_3}^0$ is carbon mols of glycerol in the feed, $C_{\text{C}_3\text{H}_8\text{O}_3}$ is carbon mols of glycerol in an aliquot taken every hour, X_L is conversion to liquid, C_{Acetol} , $C_{\text{Propyleneglycol}}$, C_{Ethanol} , C_{Acrolein} are carbon mols of acetol, propylene glycol, ethanol, and acrolein, S_i^l is the selectivity of each liquid product and Y_i^l is the yield of each liquid product.

Turnover frequencies (TOF) values were calculated based on propylene glycol formation on the sixth hour of reaction, using the glycerol conversion to liquid and selectivity to propylene glycol, and the metallic dispersions displayed in Table 1.

$$\text{TOF (h}^{-1}\text{)} =$$

$$\frac{\text{Glycerol feed molar flow (mol h}^{-1}\text{)} \times X_L(\%) \times S_{\text{propyleneglycol}}^l(\%)}{\text{surface active sites (mol)}} \quad (7)$$

As only one measurement of conversion and selectivity was used to calculate TOF (6 h of reaction, at 250°C and 40 bar of N_2), some authors prefer to use the term site-time yield (STY) [18,19].

3. Results and discussion

3.1. Catalyst characterization

Table 1 shows that the real chemical composition of the catalysts is very close to the theoretical values and small differences can be explained by the uncertainty of measurement of X-ray fluorescence. According to the XRF analysis, ZSM-5 has a $\text{SiO}_2/\text{Al}_2\text{O}_3$ molar ratio equal to 11, which corresponds to a weight composition of 86% SiO_2 and 14% Al_2O_3 .

Fig. 1(A–F) shows the XRD patterns of the calcined, reduced, and spent catalysts, as well as their respective supports. $\text{CuNi}/\text{Al}_2\text{O}_3$ calcined catalyst presented characteristic peaks of NiO at 37.3° , 43.2° and 62.9° (JCPDS 44-1159), CuO at 35.2° , 38.4° and 48.8° (JCPDS 44-0706) and also the characteristic support structure ($\gamma\text{-Al}_2\text{O}_3$). $\text{CuNi}/\text{ZSM-5}$ calcined catalyst exhibited the same peaks of NiO and CuO , in addition to the characteristic peaks of the support (ZSM-5) (JCPDS 44-0002). The peaks obtained for the impregnated catalyst were almost the same as that of pure ZSM-5, indicating that the support retained the primary structure after the loading process [20,21]. The monometallic catalysts presented only the characteristic peaks of CuO or NiO and the support.

In order to characterize the catalysts after reduction, a reduction temperature of 550°C was chosen for Cu-containing catalysts, or 850°C , for Ni monometallic catalysts, according to TPR analysis. XRD patterns of the reduced catalysts are shown in Fig. 1 and a more detailed comparison is displayed in Fig. S1 of the Supplementary Material. The reduction of monometallic catalysts resulted in the formation of metallic Cu at 43.2° , 50.4° and 74.1° (JCPDS 04-0836) or Ni at 44.5° , 51.8° and 76.4° (JCPDS 04-0850). For bimetallic catalysts, peaks are observed at intermediate positions between the metallic Ni and Cu, thus the copper is forming an alloy with nickel [22,23]. In the case of $\text{CuNi}/\text{ZSM-5}$ the presence of two peaks at intermediate position (see Fig. S3) shows that there is an alloy more enriched in Ni, which is predominant, and another one enriched in Cu. Experimental lattice parameters of the metallic phase, obtained from XRD patterns of the reduced catalysts and displayed in Table 1 (and also Tables S1 and S2), showed that bimetallic catalysts presented intermediate values between nickel and copper, which have FCC structure with lattice parameter $a = 3.524 \text{ \AA}$ and 3.615 \AA , respectively. The actual composition of the $\text{Ni}_{x}\text{Cu}_{1-x}$ alloy can be calculated applying the Vegard's law ($a_{\text{Ni}_{x}\text{Cu}_{1-x}} = x \cdot a_{\text{Ni}} + (1-x) \cdot a_{\text{Cu}}$) [24,25]; the values are shown in Tables S1 and S2. The Ni composition of the alloy is very close to the nominal composition in both catalysts; in the case of $\text{CuNi}/\text{ZSM-5}$ catalyst, the sum of Ni content of the two different alloys (considering the areas obtained from deconvolution of the (111) peak) is equivalent to total Ni loading.

The catalysts supported on ZSM-5 presented the same phases after reaction as those after reduction, but with small changes in Ni–Cu alloy composition (Table S2). On the other hand, there was formation of a new crystalline phase of boehmite (AlOOH), with main reflections at 14.4° , 28.1° , 38.3° , 48.9° , and 71.9° (JCPDS 21-1307), for Ni and $\text{Cu}/\text{Al}_2\text{O}_3$, as also observed by Wen et al. [26] for $\text{Ni}/\text{Al}_2\text{O}_3$ catalysts after aqueous-phase reforming of glycerol at 230°C . It was also observed boehmite formation when pure alumina was tested under the same reaction conditions. It is known in the literature [27,28] that the presence of metal particles retards the transformation of γ -alumina into boehmite, and our results point out that this effect is more severe with increasing metal loading, which explains why boehmite was not observed in the bimetallic catalyst. The active metallic phase of the catalyst was maintained in its reduced state after the reaction, without diffraction peaks related to the CuO/NiO phase, showing the good stability of the reduced metals under reaction conditions used here. Yun et al. [13]

Table 1

Chemical composition of the calcined Cu-Ni catalysts, Ni⁰, Cu⁰ and Cu⁰/Ni⁰ crystallite sizes of reduced and spent catalysts, metallic dispersion (D) and lattice parameters (*a*) of the metal phase on reduced catalysts.

Catalyst	CuO (wt%)	NiO (wt%)	Crystallite size (nm) ^a		D (%)	<i>a</i> (Å)
			Reduced	Spent		
Cu/Al ₂ O ₃	22	–	22.3 (±2.3)	26.6 (±1.2)	4.7	3.6156
Ni/Al ₂ O ₃	–	19	7.4 (±1.9)	10.0 (±1.4)	14.0	3.5244
CuNi/Al ₂ O ₃	22	19	6.0 (±0.2)	7.9 (±0.2)	17.1	3.5692
Cu/ZSM-5	19	–	27.6 (±1.7)	31.0 (±3.6)	3.8	3.6143
Ni/ZSM-5	–	22	24.2 (±1.7)	25.6 (±2.1)	4.0	3.5224
CuNi/ZSM-5	19	22	16.0 (±0.8)	18.6 (±1.0)	6.4	3.5618 ^b

^a Calculated by the Scherrer equation.

^b Mean value of Ni-rich and Cu-rich phases (see Table S2).

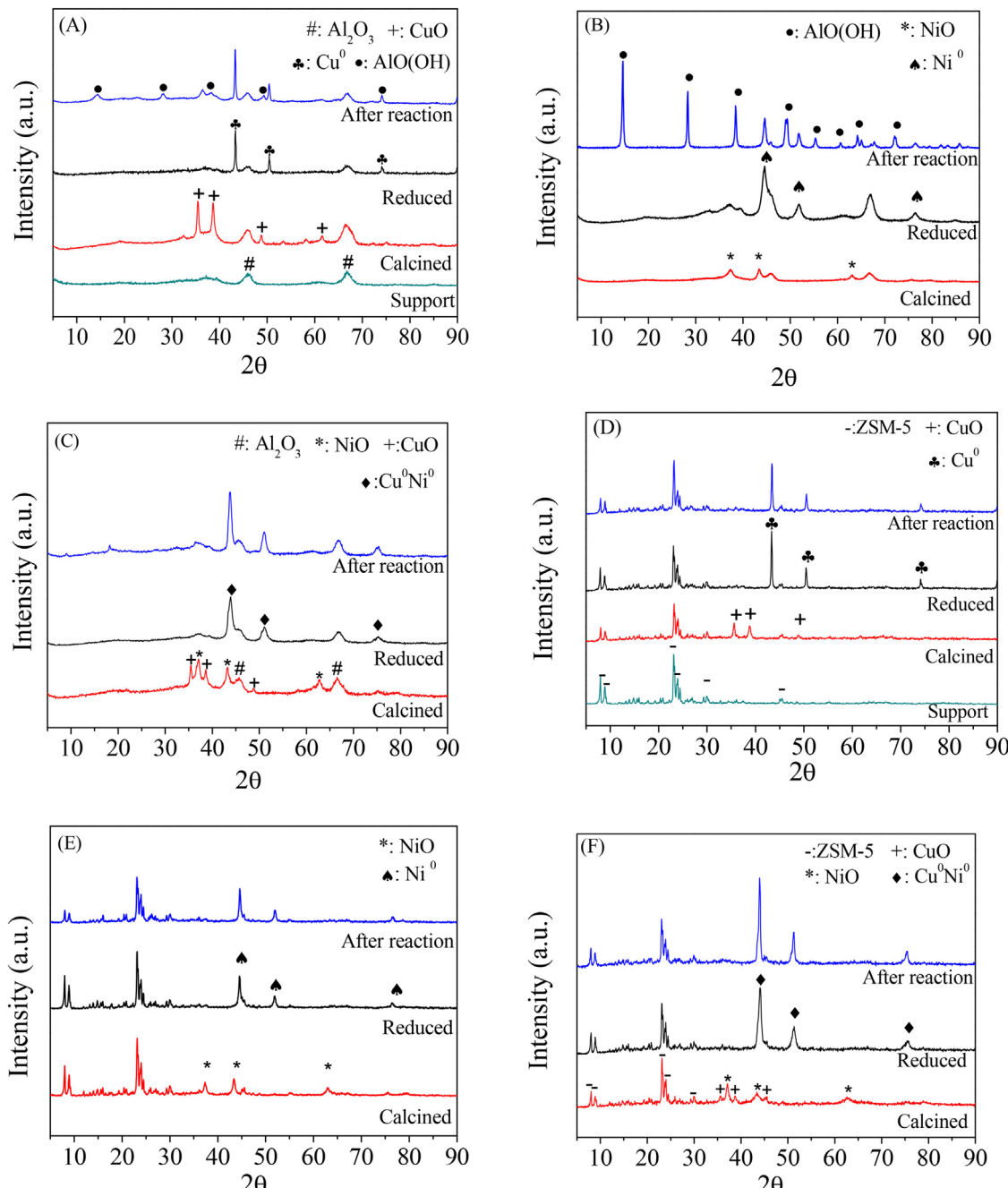


Fig. 1. XRD patterns of the catalysts after calcination, reduction and after reaction: (A) Cu/Al₂O₃, (B) Ni/Al₂O₃, (C) CuNi/Al₂O₃, (D) Cu/ZSM-5, (E) Ni/ZSM-5 and (F) CuNi/ZSM-5.

observed that reduced metallic copper was oxidized during glycerol hydrogenolysis after 12 h of reaction in a batch reactor at 220 °C.

According to Table 1, there was a decrease in the metallic crystallite size with addition of the second metal, for both catalysts supported on ZSM-5 and Al₂O₃. The same tendency was observed by Manfro et al. [23] for Ni-Cu catalysts derived from hydrotalcite precursors and by Wang et al. [29] for alumina supported catalysts (the average crystallite size was 25.1 nm for 2Cu/Al₂O₃ and 13.2 nm for 2Cu-1Ni/Al₂O₃ catalyst). The crystallite sizes after reaction are similar to those before reaction, showing that sintering was not a critical problem for these catalysts. The metallic dispersion is greater for bimetallic catalysts and, although ZSM-5 has larger BET surface area than alumina, the catalysts supported on ZSM-5 presented lower dispersion.

X-ray photoelectron spectroscopy (XPS) analysis of the bimetallic catalysts was employed to obtain detailed information on the Ni and Cu surface composition and their oxidation states in the reduced samples. Table 2 displays a summary of XPS results, and Figs. S4 and S5 show the high resolution spectra of Cu2p and Ni2p photoelectron lines for CuNi/Al₂O₃ and CuNi/ZSM-5 catalysts, respectively. Ni/Cu surface atomic ratio is close to the bulk value for Al₂O₃ catalyst, and slightly higher for ZSM-5 catalyst, showing a certain degree of Ni enrichment on the surface. According to Gervasini [30] copper ions penetrate to a greater extent in the channels of ZSM-5 zeolite than nickel ions, which can be related to the lower Cu content on the surface of CuNi/ZSM-5 catalyst.

The Cu2p_{3/2} spectra of these catalysts can be divided into two peaks: at 932.1–932.4 eV, assigned to metallic Cu, and at 932.9–934.4 eV, associated with Cu²⁺ in CuO. The binding energy (BE) values for Cu are very close to that expected for Cu metal (932–932.9 eV) but the BE value of Cu²⁺ for CuNi/ZSM-5 is slightly lower (933.2–934.6 eV) [31,32]. Thus, the interaction of Cu²⁺ ions with the zeolite structure modifies their electronic distribution to some extent. The Ni2p_{3/2} spectra can also be divided into two: at 852.7–853.8 eV, related to metallic Ni, and at 855.4–856.5 eV, associated with Ni²⁺ in NiO. These BE values related to metallic Ni are a bit higher than those expected for bulk nickel [31]. Variations from +0.8 to +1 eV were found in the experimental Ni2p_{3/2} BE of nickel in the Cu-Ni alloys by Naghash et al. [33], which was attributed to the Ni-Ni arrangements in the solid solution and to nickel-copper d-d band interactions. In our case, we cannot associate these variations in the BE values only to alloy formation, because we did not study different alloy compositions on the same support, and the support plays a very important role on the chemical states of nickel and copper. In general, the BE shifts associated with Cu-Ni alloy formation are lower than ±0.2 eV [32,34]. It is worth noting, however, that the metallic Cu and Ni ratios on the surface of CuNi/Al₂O₃ catalyst are much higher than on CuNi/ZSM-5 (Table 2), showing that oxide species are predominant on the surface of this last catalyst. No oxide species were detected on XRD analyses after reduction, indicating that these species are well dispersed on the surface. The lower reduction degree of CuNi/ZSM-5 was observed by TPR, as it will be shown in Table 3.

Fig. 2 shows the FTIR analysis of ZSM-5 pure and impregnated with Ni and Cu. The major bands at 1230, 1100 and 796 cm⁻¹ represent the Si—O—Si bonds of zeolitic structure and the band at 1637 cm⁻¹ is associated with H—O—H bonds. The absorption bands around 543 and 450 cm⁻¹ are characteristic of the crystalline structure of ZSM-5 [35].

Table 3 shows the textural analysis of the catalysts, which was performed by N₂ physisorption. For both supports, the metal addition decreases the BET area and pore volume, as Cu-Ni particles may block the pores of the support during metal deposition. The isotherms of the alumina supported catalysts exhibited type IV pattern with H1 hysteresis loop, which are typical of mesoporous materials, with pores ranging from 2 to 50 nm.

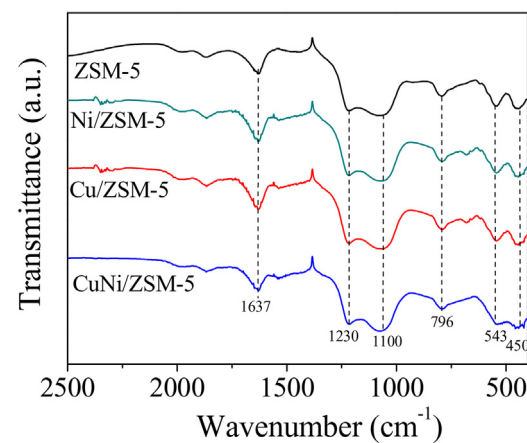


Fig. 2. FTIR spectra of the ZSM-5 catalysts.

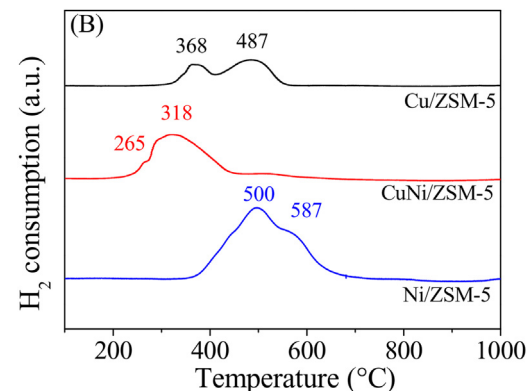
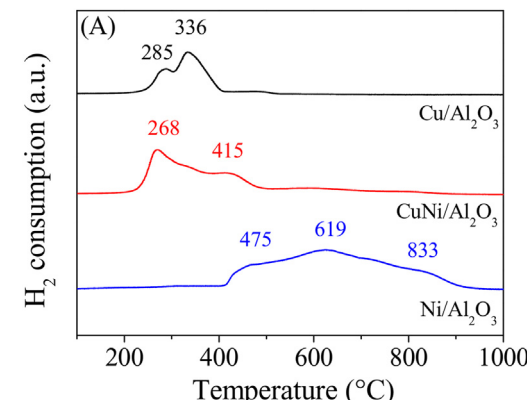


Fig. 3. TPR profiles of the catalysts supported on (A) Al₂O₃ and (B) ZSM-5.

ZSM-5 support has a much larger BET surface area than alumina, but with lower pore volume. The BET area found here for ZSM-5 is very close to the value reported by Ji et al. (354 m² g⁻¹) [20] and Gervasini (372 m² g⁻¹) [30]. The isotherms of the ZSM-5 supported catalysts exhibited type II pattern with H3 hysteresis loop, which are typical of microporous materials, with pores smaller than 2 nm.

Fig. 3 shows the reduction profiles of the catalysts, while Table 3 presents the reduction degree of CuO and NiO of the supported catalysts. For bimetallic catalysts, a total reduction degree was calculated for both CuO and NiO because of peak overlapping. The Cu/Al₂O₃ catalyst presented two reduction peaks, at 285 °C and 336 °C. Both reduction peaks correspond to the reduction of Cu²⁺ to Cu⁰, since pure CuO has a reduction temperature in the range of 200–400 °C [36]. The reduction peak in the lower temperature may be attributed to reduction of the copper dispersed on the catalyst

Table 2

Summary of XPS results of the bimetallic catalysts after reduction: Ni/Cu surface atomic ratio, binding energies of Cu $2p_{3/2}$ for Cu 0 and Cu $^{2+}$ species and Ni $2p_{3/2}$ for Ni 0 and Ni $^{2+}$ species.

Catalyst	Ni/Cu bulk ratio ^a	Ni/Cu surface ratio	Cu 0 (eV)	Cu $^{2+}$ (eV)	Ni 0 (eV)	Ni $^{2+}$ (eV)	Cu 0 /(Cu 0 +Cu $^{2+}$)	Ni 0 /(Ni 0 +Ni $^{2+}$)	Ni 0 /Cu 0 surface ratio
CuNi/Al $_2$ O $_3$	0.9	0.82	932.4	934.4	853.8	856.5	0.59	0.76	1.05
CuNi/ZSM-5	1.2	1.47	932.1	932.9	852.7	855.4	0.28	0.31	1.65

^a Calculated from XRF results.

surface, which has a weak interaction with the support, and the reduction peak at the highest temperature might be attributed to the reduction of the bulk CuO [7]. The Ni/Al $_2$ O $_3$ presented a large reduction peak that may be deconvoluted into three, at 475, 619 and 833 °C, which are related to the reduction of NiO with strong interaction with the support, because pure NiO reduces at 300–420 °C [37]. The CuNi/Al $_2$ O $_3$ catalyst presented two reduction peaks, the first (268 °C) is related mainly to the reduction of CuO, while the second (415 °C) corresponds to the reduction of NiO [36,38]. The presence of Cu species strongly promotes the NiO reduction, causing a decrease in its reduction temperature [39] and the opposite is also valid since the temperature of the first reduction peak of CuO was decreased in the bimetallic catalyst [38,40].

For Cu/ZSM-5 catalyst, there were two reduction peaks, at 368 and 487 °C, which can be attributed to the reduction of copper in two steps, from Cu $^{2+}$ to Cu $^+$ and from Cu $^+$ to Cu 0 , respectively [41]. Two reduction peaks at 500 and 587 °C were observed for Ni/ZSM-5 catalyst, in accordance with Mohan et al. [35], who observed a reduction peak at about 500 °C. The CuNi/ZSM-5 catalyst also showed two reduction peaks, at 265 and 318 °C; it is difficult to attribute the contribution of each metal phase to each peak because of peak overlapping. The decrease of reduction temperature of NiO by the presence of CuO is due to both a synergistic interaction between the metallic oxide phases and a decrease of its crystallite size [42]. Reduction degree (Table 3) was 100% only for Cu/ZSM-5 showing that there are oxide species in the reduced catalysts, and these species are mainly on the catalyst surface (they were clearly observed on XPS analysis but not on XRD patterns).

NH $_3$ desorption profiles of the catalysts supported on Al $_2$ O $_3$ and ZSM-5 are shown in Fig. 4. The Al $_2$ O $_3$ catalysts (Fig. 4A) showed an intense peak of desorption around 220 °C and a small one at 450 °C, while for the ZSM-5 supported catalysts (Fig. 4B) there were two ranges of desorption temperatures, the first at 150–400 °C and the second between 400 and 650 °C. The first peak is associated with weak acid sites and the second related to the strong acid sites [43,44].

According to Table 3, it can be seen that catalysts supported on ZSM-5 showed high acidity compared with catalysts supported on Al $_2$ O $_3$. The catalysts supported on alumina showed NH $_3$ desorption between 315 and 350 μmolNH $_3$ g $_{cat}^{-1}$, in accordance with the values reported by Gandarias et al. [7], while the catalysts supported on ZSM-5 showed values between 615 and 660 μmolNH $_3$ g $_{cat}^{-1}$, close to that reported by Vennestrøm et al. [45]. There was a small

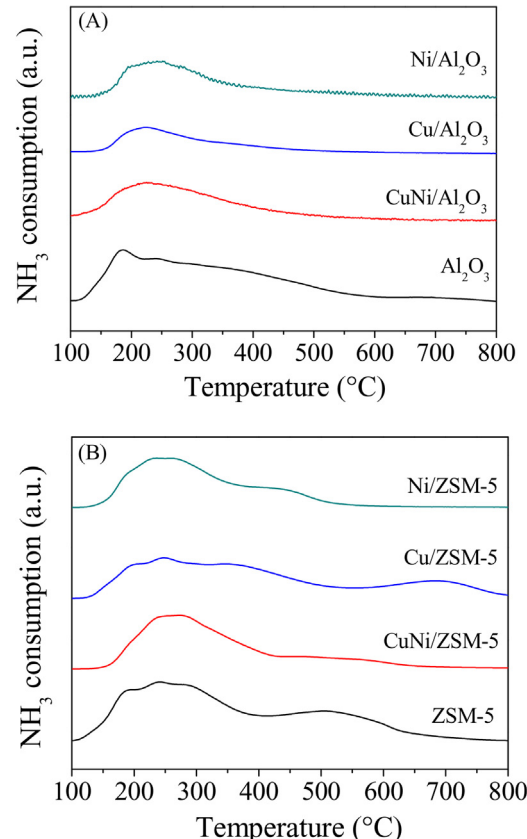


Fig. 4. NH $_3$ -TPD profiles of the catalysts supported on (A) Al $_2$ O $_3$ and (B) ZSM-5.

Table 3

Textural properties, reduction degrees (RD) of CuO and/or NiO calculated from TPR results and amount of desorbed NH $_3$, proportion of weak and high strength acid sites, and density of acid sites derived from NH $_3$ -TPD profiles.

Catalyst	S _{BET} (m 2 g $^{-1}$)	V _{pore} (cm 3 g $^{-1}$)	RD (%) ^a	μmol NH $_3$ g $_{cat}^{-1}$	Ratio of weak:high strength acid sites ^b (%)	μmol NH $_3$ m $^{-2}$
Al $_2$ O $_3$	193	0.70	–	362	27:73	1.88
Cu/Al $_2$ O $_3$	152	0.55	85	349	48:52	2.30
Ni/Al $_2$ O $_3$	137	0.43	98	325	60:40	2.37
CuNi/Al $_2$ O $_3$	128	0.42	84	317	39:61	2.47
ZSM-5	400	0.13	–	681	58:42	1.70
Cu/ZSM-5	231	0.09	100	659	71:29	2.85
Ni/ZSM-5	235	0.05	76	638	55:45	2.71
CuNi/ZSM-5	184	0.06	78	616	62:38	3.35

^a Reduction degree (%) = H $_2$ uptake (experimental)/H $_2$ uptake (theoretical) × 100, considering H $_2$ total uptake for bimetallic catalyst.

^b Calculated from Gaussian deconvolution of NH $_3$ -TPD profiles (weak: below 400 °C; high: above 400 °C).

decrease of the amount of acid sites for all catalysts when compared to the bare supports, due to partial covering of acid sites by metal clusters. Although the total amount of acid sites of ZSM-5 catalysts is higher than Al $_2$ O $_3$ catalysts, the density of acid sites (in μmolNH $_3$ m $^{-2}$) is similar, due to the larger BET surface area of ZSM-5.

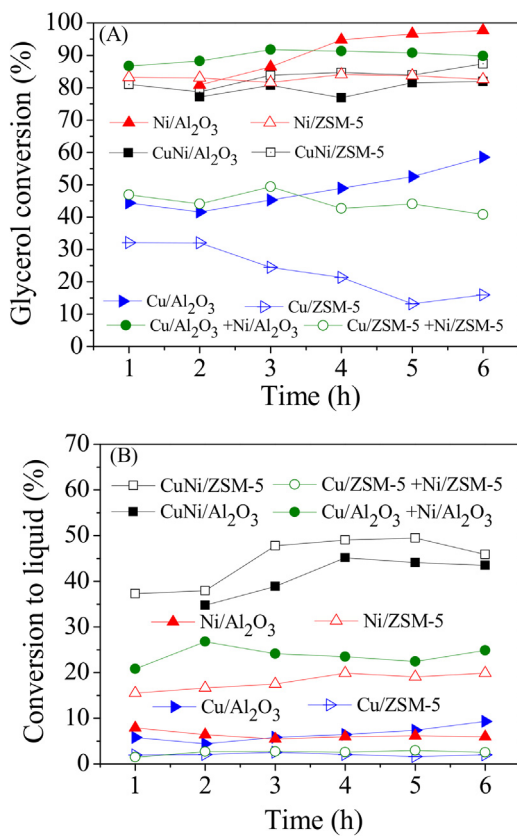


Fig. 5. Glycerol conversion (A) and conversion to liquid (B) with Cu-Ni catalysts at 250 °C, under 40 bar of N₂ pressure.

3.2. Activity tests

3.2.1. Activity tests without external hydrogen

Fig. 5 shows the glycerol conversion and conversion to liquids obtained in activity tests performed at 250 °C, under 40 bar of N₂ pressure. The Ni/Al₂O₃ catalyst presented the highest glycerol conversion, reaching 98% (Fig. 5A). In relation to bimetallic catalysts, CuNi/ZSM-5 catalyst presented glycerol conversion of approximately 85%, very close to that of CuNi/Al₂O₃ catalyst (80%). When comparing conversion to liquid (Fig. 5B), CuNi/ZSM-5 catalyst exhibited the highest conversion, around 50%, followed by CuNi/Al₂O₃ catalyst (40%). The Ni/ZSM-5 exhibited about 20% of conversion to liquid (mainly ethanol, as it will be seen later), against only 6% for Ni/Al₂O₃. The high glycerol conversion of Ni monometallic catalysts and low conversion to liquid confirm the high activity of these catalysts for glycerol reforming at this temperature. The gas phase for Ni monometallic catalysts contained approximately 50%H₂, 40%CO₂ and 10%CH₄, and for bimetallic catalysts the H₂ molar fraction was lower.

The monometallic Cu catalysts presented low glycerol conversion, especially that supported on ZSM-5 (15% after 6 h), and the conversion to liquid was only 9% for the Cu/Al₂O₃ catalyst and lower than 2% for the Cu/ZSM-5 catalyst. The very low conversion to liquids shows that copper catalysts are also active for glycerol reforming to H₂ and CO₂ [15], as shown by GC analysis, although less active than Ni for this reaction [7].

Physical mixtures of the monometallic catalysts were also evaluated, in order to analyze the effect of Ni-Cu alloy on the catalyst activity. The physical mixture of alumina supported catalysts showed high glycerol conversion, close to Ni/Al₂O₃, and the conversion to liquid was about 24%, much lower than CuNi/Al₂O₃ catalyst. In the case of the physical mixture of ZSM-5 supported catalyst, the

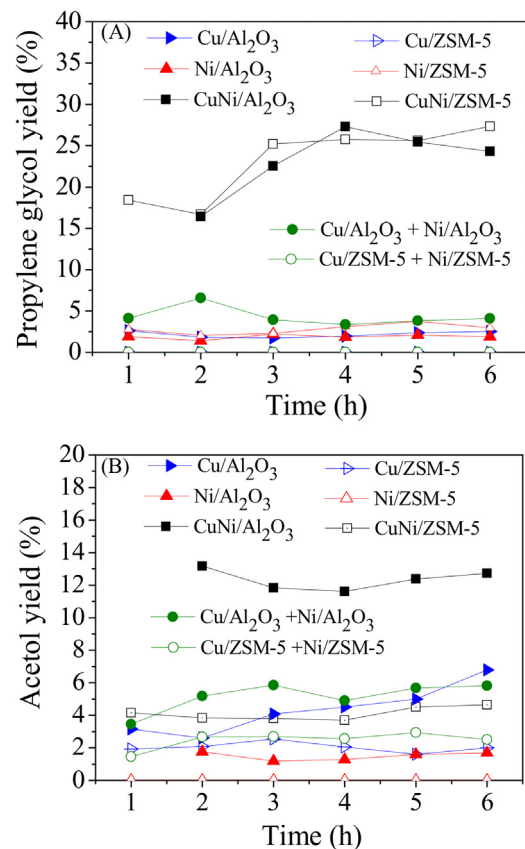


Fig. 6. Propylene glycol (A) and acetol (B) yield with Cu-Ni catalysts at 250 °C, under 40 bar of N₂ pressure.

conversion to liquid was even lower (only 2.5%). Thus, the interaction of Ni and Cu on bimetallic catalysts is essential for increasing the activity towards hydrogenolysis reaction.

Fig. 6 shows the yields to propylene glycol and acetol, the main products of glycerol hydrogenolysis under the reaction conditions used here. The bimetallic catalysts exhibited the highest propylene glycol yields, with values around 25%. Considering that acetol yield is much higher for CuNi/Al₂O₃, the conversion of acetol to propylene glycol is faster on CuNi/ZSM-5, which may be related to higher activity of this catalyst for H₂ formation from glycerol reforming.

For monometallic catalysts, the Cu/Al₂O₃ showed a very low propylene glycol yield (around 2%), close to Ni catalysts, and the Cu/ZSM-5 did not show any formation of the product of interest. The acetol yield is also low for these catalysts, with maximum of approximately 6% for Cu/Al₂O₃. The physical mixture of alumina catalysts showed low propylene glycol yield (4%), while for ZSM-5 catalysts there was no detectable formation of propylene glycol. This is a good evidence of the role of NiCu alloy on bimetallic catalysts for propylene glycol formation.

As the acidity of monometallic and bimetallic catalysts is very similar, the dehydration of glycerol to acetol cannot be associated only with acid sites. Our control experiments showed that pure Al₂O₃ and ZSM-5 did not give detectable glycerol conversion, suggesting that the metal sites are prerequisite for the reaction, as also shown in the literature [46–48]. The necessity to have a good balance between the two catalytic functions (acid and metal sites) for hydrogenolysis of glycerol has already been observed by other authors [10,48,49]. Cai et al. [49] reported a linear correlation between glycerol conversion and acidity of Cu-ZrO₂-Al₂O₃ catalysts, while a direct correlation was established between propylene glycol yield and Cu dispersion. In our case a direct correlation of

Table 4

Comparison between our results and other works in the literature that also studied glycerol hydrogenolysis in the absence of external hydrogen.

Catalyst	Pressure (bar)	Temperature (°C)	Time (h)	Glycerol conversion (%)	Propylene glycol selectivity (s) or yield (y) (%)	Ref.
3.0Pt/Al ₂ O ₃ ^a	n.r.	230	24	99.9	19.1 (s)	[11]
5Ru/Al ₂ O ₃ + 5Pt/Al ₂ O ₃ ^a	14	220	6	50.1	47.2 (s)	[12]
7Cu-3Ni/Al ₂ O ₃ ^a	1	220	10	60	20 (y)	[13]
65Ni/SiO ₂ -Al ₂ O ₃ ^a	33.5	240	4	80	22 (y)	[14]
50Cu-Al ^b LHSV = 1.53 h ⁻¹	20	220	400	90	25 (s)	[15]
CuNi/Al ₂ O ₃ ^b WHSV = 2 h ⁻¹	40	250	6	82	24 (y)	This work
CuNi/ZSM-5 ^b WHSV = 2 h ⁻¹	40	250	6	87	27 (y)	This work

n.r. = not reported.

^a Batch reactor.

^b Fixed bed reactor.

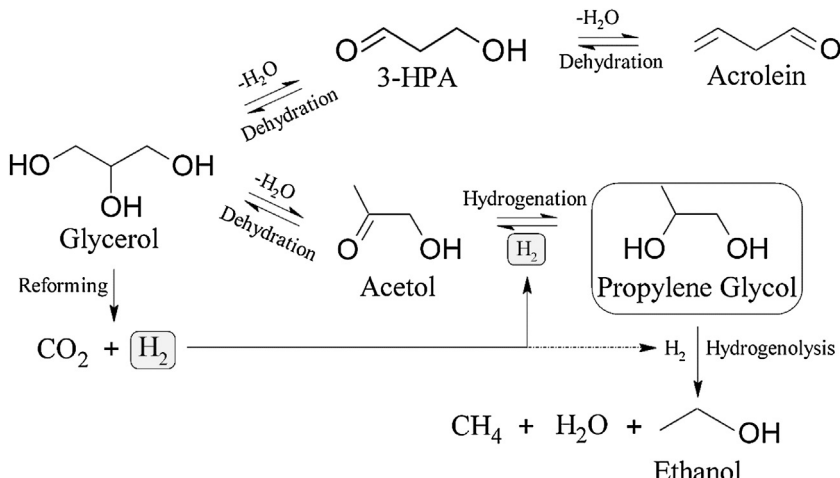


Fig. 7. Proposed reaction mechanism for the glycerol hydrogenolysis.

metallic dispersion with propylene glycol yield cannot be observed, because of different acidity of the supports.

The ethanol formation was observed only for the Ni-containing catalysts, with yield of 3% for Ni/Al₂O₃, against 17% for Ni/ZSM-5. The absence of ethanol formation for Cu monometallic catalysts indicates the lower activity of Cu catalysts for the cleavage of C–C bond [13,50]. Table S3 summarizes the results of conversion, selectivity and yield in the sixth hour of reaction.

Table 4 shows a comparison between our results and other works in the literature that also studied glycerol hydrogenolysis in the absence of external hydrogen. It can be clearly seen that the results of bimetallic catalysts in terms of glycerol conversion and propylene glycol yield are similar to other reports, especially that of Mane and Rode [15], who also used fixed bed reactor.

The following order of TOF (calculated according to Eq. (7)) was obtained: CuNi/ZSM-5 (7.1 h⁻¹) ≫ CuNi/Al₂O₃ (1.7 h⁻¹) > Ni/ZSM-5 (1.5 h⁻¹) ≈ Cu/Al₂O₃ (1.4 h⁻¹) > Ni/Al₂O₃ + Cu/Al₂O₃ (1.1 h⁻¹) > Ni/Al₂O₃ (0.2 h⁻¹) > Cu/ZSM-5 (0) = Ni/ZSM-5 + Cu/ZSM-5 (0). Although the reaction rates for bimetallic catalysts were almost the same, the higher dispersion of CuNi/Al₂O₃ decreased its TOF. It is very difficult to compare these values of TOFs with others in the literature, because most of the studies were carried out in batch reactor and H₂ pressure. The higher TOF obtained by Xia et al. [51] was 18.1 h⁻¹ for Pd-Cu catalysts, at 180 °C and 2.0 MPa of H₂, while Wang et al. [52] reported a TOF of 1.3 h⁻¹ for Ru/Al₂O₃ catalyst, at 200 °C and 6.0 MPa of H₂.

The proposed reaction mechanism for the glycerol hydrogenolysis is shown in Fig. 7. Firstly the glycerol is dehydrated to acetol, which is assumed to occur preferentially in acid sites [4,53–55], and simultaneously reformed to H₂ and CO₂, in metal sites. This hydrogen generated *in situ* is used for the hydrogenation of acetol to form

propylene glycol, in metal sites. Ethanol can be produced from the hydrogenolysis of propylene glycol [53,56] and acrolein if formed by excessive dehydration of glycerol [8,57]. Glycerol can dehydrate through two distinct and independent pathways, as shown in Fig. 7: one leading to acetol and the other forming acrolein, through 3-hydroxypropenal (3-HPA), a very unstable product (not detected by HPLC). The first pathway implies the removal of one of the two terminal alcohol groups in the glycerol molecule, whereas the second implies the removal of the central alcohol function [58,59].

3.2.2. Activity tests with external hydrogen

The catalysts were also evaluated in the glycerol hydrogenolysis with addition of external hydrogen, in order to compare the effect of inert/reactive atmosphere on catalytic activity and reaction pathway. Monometallic Ni catalysts were not evaluated in this case because the primary role of Ni sites is in glycerol reforming for hydrogen production, and in the presence of external hydrogen the reforming reaction is hindered.

The addition of H₂ caused an increase in glycerol conversion for all the catalysts, with values above 90%, according to Fig. 8A. The conversion to liquid (Fig. 8B) increased for the CuNi/Al₂O₃ catalyst, with values around 70%, while for the CuNi/ZSM-5 catalyst the values were around 35%, lower than that without external hydrogen, showing a greater formation of gaseous products in this case. The higher conversion to gaseous products can be related to CH₄ formation by glycerol degradation, which was directly correlated with acidity of HSZM-5 supported catalysts by Li et al. [60]. Indeed, CH₄ was the main gas product detected in this case. Delgado et al. [55] also observed that a too high quantity of acid sites promotes C–C bond cleavage via cracking mechanism, with formation of C₁–C₃ hydrocarbons.

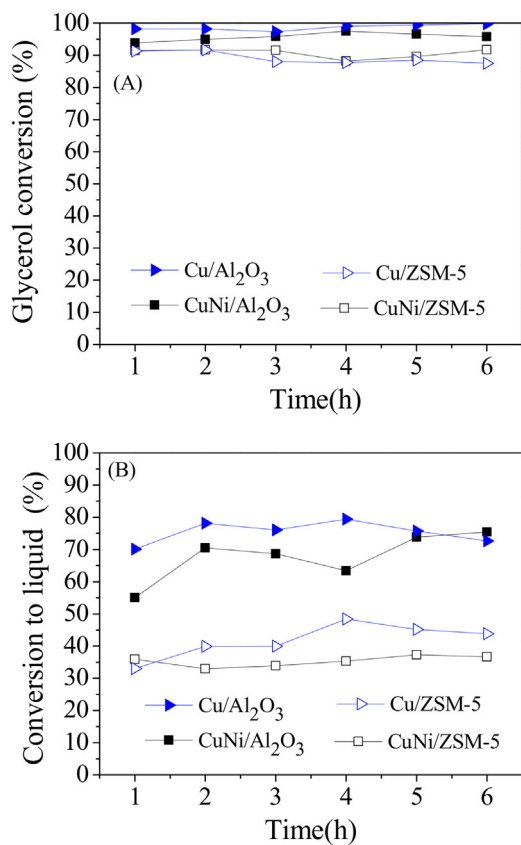


Fig. 8. Glycerol conversion (A) and conversion to liquid (B) with Cu-Ni catalysts at 250 °C, under 40 bar of H₂ pressure.

The Cu monometallic catalysts presented higher conversion to liquid than the correspondent bimetallic ones: 75% for Cu/Al₂O₃ and 40% for the Cu/ZSM-5 catalyst. Thus, under high pressure of hydrogen, the addition of Ni is not making difference for glycerol conversion, which confirms that the main role of Ni sites is in glycerol reforming under inert atmosphere [13,61]. With addition of external hydrogen, the reforming reaction should have the equilibrium shifted towards reactants; the formation of H₂ in general is not observed when the system is pressurized with hydrogen [53,61].

The propylene glycol and acetol yields with addition of external hydrogen can be seen in Fig. 9. Concerning the acetol yields, the values are close to those obtained without hydrogen: 10% for CuNi/Al₂O₃, 4% for CuNi/ZSM-5 catalyst, and around 5% for the Cu monometallic catalysts.

The main effect expected when adding hydrogen was to increase the propylene glycol yield, due to enhancement of hydrogenation of acetol. This effect can be clearly seen for Cu monometallic catalysts: the Cu/Al₂O₃ catalyst had the highest propylene glycol yield, with values around 70%, and 30% for Cu/ZSM-5, while formation of propylene glycol was almost null in the absence of hydrogen for both catalysts. For CuNi/Al₂O₃ catalyst the propylene glycol yield also increased, from around 25% to 50%. However, for CuNi/ZSM-5 catalyst the propylene glycol yield was 25%, the same as that without external hydrogen.

The better performance of alumina-supported catalysts for propylene glycol formation can be related to the higher Cu dispersion on these catalysts (Table 1), since Cu metal sites are directly involved in the hydrogenation step of acetol to propylene glycol. A direct correlation between dispersion of Cu species and the activity for propylene glycol formation was established by Zhou et al. [61] for Cu-Ag/Al₂O₃ catalyst and also by Yuan et al. [53] for Cu_{0.4}/Mg_{5.6}Al₂O_{8.6} catalyst, using external H₂ in a batch reactor.

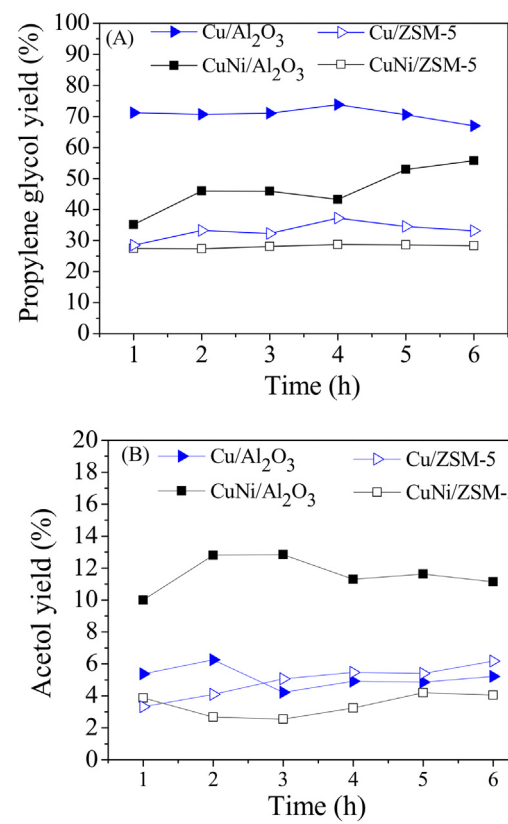


Fig. 9. Propylene glycol (A) and acetol (B) yield with Cu-Ni catalysts at 250 °C, under 40 bar of H₂ pressure.

The lower values of propylene glycol yield for ZSM-5 catalysts can also be associated with their high acidity, making the glycerol dehydrate to acrolein and not to acetol, as also observed by Guo et al. [8]. Indeed, it was detected presence of acrolein with yield around 5% for the Cu/ZSM-5 catalyst. Table S4 summarizes the results of conversion, selectivity and yield in the sixth hour of reaction, in the presence of hydrogen.

In relation to ethanol yields, the bimetallic catalysts showed values around 4–8%, while the monometallic catalysts did not show any formation of ethanol. Balaraju et al. [62] pointed that the optimum temperature for propylene glycol formation over Cu-MgO catalysts is 200–220 °C in the presence of H₂, because higher temperatures leads to excessive glycerol hydrogenolysis, with formation of lower alcohols and gaseous products. However, in our case, ethanol formation is low even at 250 °C.

4. Conclusions

Cu-Ni catalysts supported on Al₂O₃ and ZSM-5 were prepared by wet impregnation, containing 20 wt% of CuO and NiO. XRD profiles showed formation of Cu-Ni alloy on bimetallic catalysts after reduction, with decrease in the metallic crystallite size and increase in the metallic dispersion. The reduction temperature of Ni species is considerably decreased by the presence of copper. The NH₃-TPD analysis showed that the catalyst supported on ZSM-5 presented a much higher acidity than the catalysts with alumina.

The catalysts were evaluated on glycerol hydrogenolysis in continuous reactor, under inert atmosphere and also in presence of hydrogen, at 250 °C. The main liquid products were always propylene glycol and acetol, with minor amounts of ethanol and acrolein. Under inert atmosphere, the glycerol conversion to liquid was much higher for the bimetallic catalysts, with propylene glycol yield around 25%, while H₂ and CO₂ are the main products for Ni

monometallic catalysts. Thus, under inert atmosphere, the presence of Ni is important for glycerol reforming, generating *in situ* H₂ that is used for acetol hydrogenation to propylene glycol. The physical mixture of Ni and Cu monometallic catalysts presented propylene glycol yield as low as the monometallic catalysts separately, showing that the Cu-Ni alloy interaction is important for the higher hydrogenolysis activity of the bimetallic catalyst. When hydrogen is added to the reaction medium, the Cu monometallic catalysts presented higher conversion to liquid and propylene glycol yield than the correspondent bimetallic ones, showing that Ni sites are not necessary in this case. The high acidity of ZSM-5 favored formation of acrolein when compared to alumina supported catalysts. The highest propylene glycol yield (70%) was obtained with Cu/Al₂O₃ using external hydrogen.

Acknowledgements

The authors thank FAPERJ, CNPq, ANP and FINEP for financial support granted to carry out this work; Fabiana M. T. Mendes of National Institute of Technology (INT) for XPS analyses; Green-tec/UFRJ and NUCAT/PEQ/COPPE/UFRJ for N₂ adsorption analyses.

Appendix A. Supplementary data

Supplementary data associated with this article can be found, in the online version, at <http://dx.doi.org/10.1016/j.apcatb.2017.08.030>.

References

- [1] S. Adhikari, S.D. Fernando, A. Haryanto, Hydrogen production from glycerin by steam reforming over nickel catalysts, *Renew. Energy* 33 (2008) 1097–1100.
- [2] F. Bauer, C. Hulteberg, Is there a future in glycerol as a feedstock in the production of biofuels and biochemicals? *Biofuels Bioprod. Biorefin.* 7 (2013) 43–51.
- [3] C.H. Zhou, J.N. Beltramini, Y.X. Fan, G.Q. Lu, Chemoselective catalytic conversion of glycerol as a biorenewable source to valuable commodity chemicals, *Chem. Soc. Rev.* 37 (2008) 527–549.
- [4] Y. Nakagawa, K. Tomishige, Heterogeneous catalysis of the glycerol hydrogenolysis, *Catal. Sci. Technol.* 1 (2011) 179–190.
- [5] Y. Nakagawa, Y. Shimmi, S. Koso, K. Tomishige, Direct hydrogenolysis of glycerol into 1,3-propanediol over rhodium-modified iridium catalyst, *J. Catal.* 272 (2010) 191–194.
- [6] E.P. Maris, R.J. Davis, Hydrogenolysis of glycerol over carbon-supported Ru and Pt catalysts, *J. Catal.* 249 (2007) 328–337.
- [7] I. Gandarias, J. Requies, P.L. Arias, U. Armbruster, A. Martin, Liquid-phase glycerol hydrogenolysis by formic acid over Ni-Cu/Al₂O₃ catalysts, *J. Catal.* 290 (2012) 79–89.
- [8] L. Guo, J. Zhou, J. Mao, X. Guo, S. Zhang, Supported Cu catalysts for the selective hydrogenolysis of glycerol to propanediols, *Appl. Catal. A Gen.* 367 (2009) 93–98.
- [9] I. Gandarias, P.L. Arias, J. Requies, M. El Doukkali, M.B. Güemez, Liquid-phase glycerol hydrogenolysis to 1,2-propanediol under nitrogen pressure using 2-propanol as hydrogen source, *J. Catal.* 282 (2011) 237–247.
- [10] Z. Wu, Y. Mao, M. Song, X. Yin, M. Zhang, Cu/boehmite: a highly active catalyst for hydrogenolysis of glycerol to 1,2-propanediol, *Catal. Commun.* 32 (2013) 52–57.
- [11] E. D'Hondt, S. Van de Vyver, B.F. Sels, P.A. Jacobs, Catalytic glycerol conversion into 1,2-propanediol in absence of added hydrogen, *Chem. Commun.* (2008) 6011–6012.
- [12] D. Roy, B. Subramaniam, R.V. Chaudhari, Aqueous phase hydrogenolysis of glycerol to 1,2-propanediol without external hydrogen addition, *Catal. Today* 156 (2010) 31–37.
- [13] Y.S. Yun, D.S. Park, J. Yi, Effect of nickel on catalytic behaviour of bimetallic Cu-Ni catalyst supported on mesoporous alumina for the hydrogenolysis of glycerol to 1,2-propanediol, *Catal. Sci. Technol.* 4 (2014) 3191–3202.
- [14] A. Seretis, P. Tsikaras, Hydrogenolysis of glycerol to propylene glycol by *in situ* produced hydrogen from aqueous phase reforming of glycerol over SiO₂-Al₂O₃ supported nickel catalyst, *Fuel Process. Technol.* 142 (2016) 135–146.
- [15] R.B. Mane, C.V. Rode, Simultaneous glycerol dehydration and *in situ* hydrogenolysis over Cu-Al oxide under an inert atmosphere, *Green Chem.* 14 (2012) 2780–2789.
- [16] T. Rajkhowa, G.B. Marin, J.W. Thybaut, A comprehensive kinetic model for Cu catalyzed liquid phase glycerol hydrogenolysis, *Appl. Catal. B Environ.* 205 (2017) 469–480.
- [17] J.R. Anderson, *Structure of Metallic Catalysts*, Academic Press, London, 1975.
- [18] M. Boudart, Turnover rates in heterogeneous catalysis, *Chem. Rev.* 95 (1995) 661–666.
- [19] T. Bligaard, R.M. Bullock, C.T. Campbell, J.G. Chen, B.C. Gates, R.J. Gorte, C.W. Jones, W.D. Jones, J.R. Kitchin, S.L. Scott, Toward benchmarking in catalysis science: best practices, challenges, and opportunities, *ACS Catal.* 6 (2016) 2590–2602.
- [20] F. Ji, C. Li, Y. Liu, P. Liu, Heterogeneous activation of peroxyomonosulfate by Cu/ZSM5 for decolorization of Rhodamine B, *Sep. Purif. Technol.* 135 (2014) 1–6.
- [21] J. Estephane, S. Aouad, S. Hany, B. El Khoury, C. Gennequin, H. El Zakhem, J. El Nakat, A. Aboukaïs, E. Abi Aad, CO₂ reforming of methane over Ni-Co/ZSM5 catalysts. Aging and carbon deposition study, *Int. J. Hydrogen Energy* 40 (2015) 9201–9208.
- [22] L. Dussault, J.C. Dupin, C. Guimon, M. Monthoux, N. Latorre, T. Ubieto, E. Romeo, C. Royo, A. Monzón, Development of Ni-Cu-Mg-Al catalysts for the synthesis of carbon nanofibers by catalytic decomposition of methane, *J. Catal.* 251 (2007) 223–232.
- [23] R.L. Manfro, T.P.M.D. Pires, N.F.P. Ribeiro, M.M.V.M. Souza, Aqueous-phase reforming of glycerol using Ni-Cu catalysts prepared from hydrotalcite-like precursors, *Catal. Sci. Technol.* 3 (2013) 1278–1287.
- [24] L. Durivault, O. Brylev, D. Reyter, M. Sarrazin, D. Bélanger, L. Roué, Cu-Ni materials prepared by mechanical milling: their properties and electrocatalytic activity towards nitrate reduction in alkaline medium, *J. Alloys Compd.* 432 (2007) 323–332.
- [25] L. De Rogatis, T. Montini, A. Cognigni, L. Olivi, P. Fornasiero, Methane partial oxidation on NiCu-based catalysts, *Catal. Today* 145 (2009) 176–185.
- [26] G. Wen, Y. Xu, H. Ma, Z. Xu, Z. Tian, Production of hydrogen by aqueous-phase reforming of glycerol, *Int. J. Hydrogen Energy* 33 (2008) 6657–6666.
- [27] R.M. Ravenelle, J.R. Copeland, W.-G. Kim, J.C. Crittenden, C. Sievers, Structural changes of γ-Al₂O₃-supported catalysts in hot liquid water, *ACS Catal.* 1 (2011) 552–561.
- [28] J. Abi Aad, Ph. Courty, D. Decottignies, M. Michau, F. Diehl, X. Carrier, E. Marceau, Inhibition by inorganic dopants of γ-Al₂O₃ chemical weathering in hydrothermal conditions: identification of reactive sites and influence in Fischer-Tropsch synthesis, *ChemCatChem* 9 (2017) 2106–2117.
- [29] X. Wang, X. Pan, R. Lin, S. Kou, W. Zou, J.X. Ma, Steam reforming of dimethyl ether over Cu-Ni/γ-Al₂O₃ bi-functional catalyst prepared by deposition-precipitation method, *Int. J. Hydrogen Energy* 35 (2010) 4060–4068.
- [30] A. Gervasini, Characterization of the textural properties of metal loaded ZSM-5 zeolites, *Appl. Catal. A Gen.* 180 (1999) 71–82.
- [31] C.D. Wagner, W.M. Riggs, L.E. Davis, J.F. Moulder, G.E. Muilenberg (Eds.), *Handbook of X-ray Photoelectron Spectroscopy*, Perkin-Elmer Corporation, 1979.
- [32] A.A. Smirnov, S.A. Khromova, O.A. Bulavchenko, V.V. Kaichev, A.A. Saraev, S.I. Reshetnikov, M.V. Bykova, L.I. Trusov, V.A. Yakovlev, Effect of the Ni/Cu ratio on the composition and catalytic properties of nickel–copper alloy in anisole hydrodeoxygenation, *Kinetics Catal.* 55 (2014) 69–78.
- [33] A.R. Naghash, T.H. Etzell, S. Xu, XRD and XPS study of Cu-Ni interactions on reduced copper-nickel-aluminum oxide solid solution catalysts, *Chem. Mater.* 18 (2006) 2480–2488.
- [34] P.F. Barbieri, A. de Sierra, M.F. Carazzolle, R. Landers, G.G. Kleiman, XPS and XAES study of Ag-Pd and Cu-Ni alloys: spectra, shifts and electronic structure information, *J. Electron Spectrosc. Relat. Phenom.* 135 (2004) 113–118.
- [35] V. Mohan, C. Raghavendra, C.V. Pramod, B.D. Raju, K.S. Rama Rao, Ni/H-ZSM-5 as a promising catalyst for vapour phase hydrogenation of levulinic acid at atmospheric pressure, *RSC Adv.* 4 (2014) 9660–9668.
- [36] L. Dussault, J.C. Dupin, E. Dumitriu, A. Auroux, C. Guimon, Microcalorimetry, TPR and XPS studies of acid-base properties of NiCuMgAl mixed oxides using LDHs as precursors, *Thermochim. Acta* 434 (2005) 93–99.
- [37] L. De Rogatis, T. Montini, B. Lorenzut, P. Fornasiero, S.E. Schwartz, D.J. Heldebrand, Ni_xCu_y/Al₂O₃ based catalysts for hydrogen production, *Energy Environ. Sci.* 1 (2008) 501–509.
- [38] B.C. Miranda, R.J. Chimentão, J. Szanyi, A.H. Braga, J.B.O. Santos, F. Gispert-Guirado, J. Llorca, F. Medina, Influence of copper on nickel-based catalysts in the conversion of glycerol, *Appl. Catal. B: Environ.* 166–167 (2015) 166–180.
- [39] Q. Guo, M. Wu, K. Wang, L. Zhang, X. Xu, Catalytic hydrodeoxygenation of algae bio-oil over bimetallic Ni-Cu/ZrO₂ catalysts, *Ind. Eng. Chem. Res.* 54 (2015) 890–899.
- [40] L. Lisi, R. Pirone, G. Russo, V. Stanzione, Cu-ZSM5 based monolith reactors for NO decomposition, *Chem. Eng. J.* 154 (2009) 341–347.
- [41] A. Vizcaíno, A. Carrero, J. Calles, Hydrogen production by ethanol steam reforming over Cu-Ni supported catalysts, *Int. J. Hydrogen Energy* 32 (2007) 1450–1461.
- [42] F. Frusteri, M. Cordaro, C. Cannilla, G. Bonura, Multifunctionality of Cu-ZnO-ZrO₂/H-ZSM5 catalysts for the one-step CO₂-to-DME hydrogenation reaction, *Appl. Catal. B Environ.* 162 (2015) 57–65.
- [43] N.F.P. Ribeiro, C.A. Henriques, M. Schmal, Copper-based catalysts for synthesis of methylamines: the effect of the metal and the role of the support, *Catal. Lett.* 104 (2005) 111–119.

- [45] P.N.R. Vennestrøm, T.V.W. Janssens, A. Kustov, M. Grill, A. Puig-Molina, L.F. Lundgaard, R.R. Tiruvalam, P. Concepción, A. Corma, Influence of lattice stability on hydrothermal deactivation of Cu-ZSM-5 and Cu-IM-5 zeolites for selective catalytic reduction of NO_x by NH₃, *J. Catal.* 309 (2014) 477–490.
- [46] X. Lin, Y. Lv, Y. Xi, Y. Qu, D.L. Phillips, C. Liu, Hydrogenolysis of glycerol by the combined use of zeolite and Ni/Al₂O₃ as catalysts: a route for achieving high selectivity to 1-propanol, *Energy Fuels* 28 (2014) 3345–3351.
- [47] A.V.-H. Soares, G. Perez, F.B. Passos, Alumina supported bimetallic Pt–Fe catalysts applied to glycerol hydrogenolysis and aqueous phase reforming, *Appl. Catal. B Environ.* 185 (2016) 77–87.
- [48] P. Hirunsit, C. Luadthong, K. Faungnawakij, Effect of alumina hydroxylation on glycerol hydrogenolysis to 1,2-propanediol over Cu/Al₂O₃: combined experiment and DFT investigation, *RSC Adv.* 5 (2015) 1188–1197.
- [49] F. Cai, W. Zhu, G. Xiao, Promoting effect of zirconium oxide on Cu–Al₂O₃ catalyst for the hydrogenolysis of glycerol to 1,2- propanediol, *Catal. Sci. Technol.* 6 (2016) 4889–4900.
- [50] R.R. Davda, J.W. Shabaker, G.W. Huber, R.D. Cortright, J.A. Dumesic, A review of catalytic issues and process conditions for renewable hydrogen and alkanes by aqueous-phase reforming of oxygenated hydrocarbons over supported metal catalysts, *Appl. Catal. B Environ.* 56 (2005) 171–186.
- [51] S. Xia, Z. Yuan, L. Wang, P. Chen, Z. Hou, Hydrogenolysis of glycerol on bimetallic Pd–Cu/solid-base catalysts prepared via layered double hydroxides precursors, *Appl. Catal. A Gen.* 403 (2011) 173–182.
- [52] S. Wang, K. Yin, Y. Zhang, H. Liu, Glycerol hydrogenolysis to propylene glycol and ethylene glycol on zirconia supported noble metal catalysts, *ACS Catal.* 3 (2013) 2112–2121.
- [53] Z. Yuan, L. Wang, J. Wang, S. Xia, P. Chen, Z. Hou, X. Zheng, Hydrogenolysis of glycerol over homogeneously dispersed copper on solid base catalysts, *Appl. Catal. B Environ.* 101 (2011) 431–440.
- [54] T. Miyazawa, Y. Kusunoki, K. Kunimori, K. Tomishige, Glycerol conversion in the aqueous solution under hydrogen over Ru/C + an ion-exchange resin and its reaction mechanism, *J. Catal.* 240 (2006) 213–221.
- [55] S.N. Delgado, D. Yap, L. Vivier, C. Espeel, Influence of the nature of the support on the catalytic properties of Pt-based catalysts for hydrogenolysis of glycerol, *J. Mol. Catal. A: Chem.* 367 (2013) 89–98.
- [56] R. Maglinao, B. He, Verification of propylene glycol preparation from glycerol via the acetol pathway by *in situ* hydrogenolysis, *Biofuels* 3 (2012) 675–682.
- [57] S. Sato, M. Akiyama, R. Takahashi, T. Hara, K. Inui, M. Yokota, Vapor-phase reaction of polyols over copper catalysts, *Appl. Catal. A: Gen.* 347 (2008) 186–191.
- [58] A. Corma, G.W. Huber, L. Sauvanaud, P. O'Connor, Biomass to chemicals: catalytic conversion of glycerol/water mixtures into acrolein reaction network, *J. Catal.* 257 (2008) 163–171.
- [59] S.-H. Chai, H.-P. Wang, Y. Liang, B.-Q. Xu, Sustainable production of acrolein: investigation of solid acid–base catalysts for gas-phase dehydration of glycerol, *Green Chem.* 9 (2007) 1130–1136.
- [60] Y. Li, L. Ma, H. Liu, D. He, Influence of HZSM5 on the activity of Ru catalysts and product selectivity during the hydrogenolysis of glycerol, *Appl. Catal. A: Gen.* 469 (2014) 45–51.
- [61] J. Zhou, L. Guo, X. Guo, J. Mao, S. Zhang, Selective hydrogenolysis of glycerol to propanediols on supported Cu-containing bimetallic catalysts, *Green Chem.* 12 (2010) 1835–1843.
- [62] M. Balaraju, K. Jagadeeswaraiah, P.S. Sai Prasad, N. Lingaiah, Catalytic hydrogenolysis of biodiesel derived glycerol to 1,2-propanediol over Cu–MgO catalysts, *Catal. Sci. Technol.* 2 (2012) 1967–1976.